Electronic structure of Bi_2Te_3 studied by angle-resolved photoemission

V. A. Greanya, W. C. Tonjes, and Rong Liu
Department of Physics and Astronomy, Michigan State University, East Lansing, Michigan 48824

C. G. Olson
Ames Laboratory and Iowa State University, Ames, Iowa 50011

D.-Y. Chung and M. G. Kanatzidis
Department of Chemistry, Michigan State University, East Lansing, Michigan 48824

(Received 31 August 2000)

We report a detailed study of the electronic structure of Bi_2Te_3, to our knowledge the best room temperature thermoelectric material known to date, using angle-resolved photoemission. Dispersions of the valence bands were determined. A sixfold *k*-space degeneracy in the valence-band maximum is found. The quasi-two-dimensional nature of the electronic structure was demonstrated by the weakly dispersive bands along the Γ-*Z* direction. Experimental results are compared with theoretical band-structure calculations and with de Haas–van Alphen and Shubnikov–de Haas experiments.

Thermoelectric materials are of interest due to their high potential for technological applications. Their ability to produce a significant temperature gradient with the application of a current (and reciprocally produce a significant current with the application of a temperature gradient) has applications in many fields such as power supply and refrigeration. Most good thermoelectric materials are narrow gap semiconductors that have a combination of high electrical conductivity, high thermopower, and low thermal conductivity.[1–5] These properties depend on aspects of the electronic structure such as the size of the band gap, the degree of *k*-space degeneracy[6] of the conduction and valence-band extrema, and their associated effective masses. Angle-resolved photoelectron spectroscopy (ARPES) is ideal to study several of these properties as it is the most direct experimental probe of the occupied bands.

In this paper, we report a detailed ARPES study of the electronic structure of Bi_2Te_3.[7] Bi_2Te_3 and its alloys are the best room-temperature bulk thermoelectric materials found to date. Recent advances in the search for new bulk thermoelectric materials rely on understanding these traditional thermoelectric materials. One of the current approaches in finding new and better thermoelectric materials is synthesizing multinary compounds using Bi_2Te_3 as a building block.[8] For example, the newly discovered $CsBi_4Te_6$ shows promising thermoelectric properties.[9]

While the transport and thermoelectric properties of Bi_2Te_3 have been extensively studied, it is only recently that the details of its electronic structure have been examined using modern band-structure calculation methods.[10,11] The calculations by Larson, Mahanti, and Kanatzidis[10] and Mishra, Satpathy, and Jepsen[11] find that the spin-orbit interaction is important in predicting the gap structure of Bi_2Te_3. They find a sixfold *k*-space degeneracy in the valence-band maximum (VBM) and a twofold *k*-space degeneracy in the conduction-band minimum (CBM). A high degree of band degeneracy is believed to contribute to a high value of thermopower. This calculation result is only partially consistent with Shubnikov–de Haas (SdH) and de Haas–van Alphen (dHvA) experiments, where a sixfold degeneracy was found for both the VBM and CBM.[12–15] In our ARPES experiments, we confirmed the sixfold degeneracy for the VBM, consistent with both the SdH and dHvA experiments and band-structure calculations. (The conduction bands are inaccessible to ARPES because they are unoccupied.) We also find the energy bands along Γ-*Z* to be weakly dispersive indicating a highly quasi-two-dimensional electronic structure.

Bi_2Te_3 is a narrow gap semiconductor with an indirect gap of approximately 0.15 eV.[16] The crystal structure is rhombohedral with the space group $D_{3d}^5(R\bar{3}m)$ with five atoms in the unit cell. The structure can be visualized as quintuple-layer leaves stacked along the *c* axis in the unit cell [Fig. 1(a)] with van der Waals bonding between the leaves. The five individual atomic layers occur in the sequence Te(1)-Bi-Te(2)-Bi-Te(1), where the Te(1) and Te(2) are nonequivalent tellurium sites.[17,18] The Brillouin zone is shown in Fig. 1(b).

The *n*-type Bi_2Te_3 crystals were grown by slow cooling of a molten Bi/Te mixture. The mixture contained $\sim$1.7% excess tellurium as a dopant, which substitutes for bismuth atoms in the crystal.[19] We also studied *p*-type Bi_2Te_3. These samples were purposely doped with additional bismuth, which substitute for tellurium atoms in the crystal. The doped samples were examined using thermopower measurements, the sign of which indicate the type of doping. ARPES measurements were carried out at the Synchrotron Radiation Center in Stoughton, Wisconsin, on the Ames-Montana ERG-Seya beam line. A movable 50 mm radius hemispherical analyzer with an angular acceptance of $\pm 1°$ was used. The energy resolution was 0.112 eV for all spectra except those along the Γ-*Z* line and those of the *p*-type sample, where the resolution was 0.068 eV. The crystals were oriented using x-ray Laue diffraction prior to being mounted in the chamber. Orientation was then confirmed by symmetry in the spectra. The crystals were cleaved in an ultrahigh vacuum ($\sim 3\times 10^{-11}$ Torr) to obtain clean surfaces. Spectra were taken at 20 K, obtained using a closed cycle helium

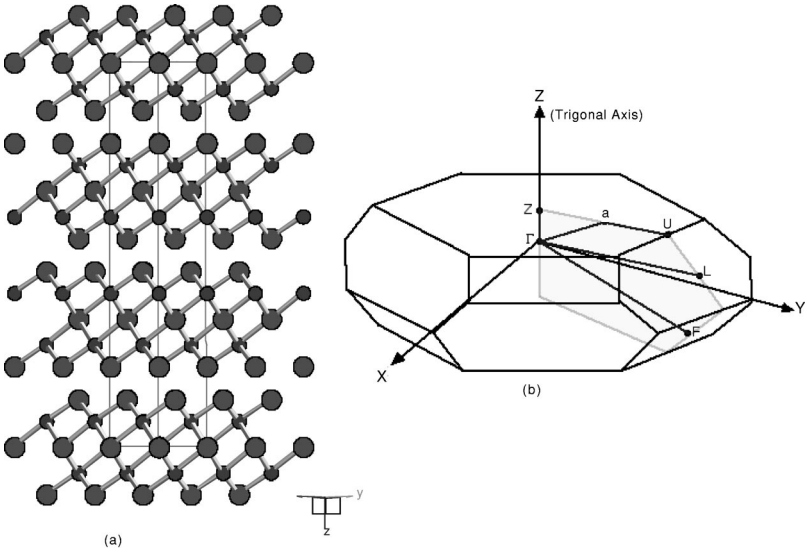

FIG. 1. (a) The crystal structure of Bi_2Te_3. The large circles are the Te atoms; the small circles are the Bi atoms. The hexagonal unit cell is indicated. (b) The Brillouin zone for Bi_2Te_3 of the rhombohedral unit cell. The shaded region is the bisectrix plane.

refrigerator, to reduce thermal broadening in the spectra.

Figure 2(a) shows the energy distribution curves (EDC's) for an *n*-type Bi_2Te_3 sample taken at normal emission (corresponding to *k* points along Γ-*Z* shown in the inset). The initial state energies were referenced to the VBM (E_{VBM}) denoted by the arrows, whose determination is explained below. As can be seen, ten bands, indicated by arrows and labeled 0 through 9, are easily identifiable in these EDC's. The features show changes in relative strength because of matrix element and cross-section effects, but significant dispersion along Γ-*Z* is not apparent. To examine the Γ-*Z* dispersions more closely, the second derivatives of the EDC's with respect to energy were obtained. Shown in Fig. 3(b) is an intensity plot of the second derivatives as a function of energy and *k* in a linear-gray scale with dark corresponding to high intensity.[20] Thus the dark areas correspond to the energy bands.[21] The intensity plot gives a direct qualitative view of the band dispersions. To get more quantitative information, the EDC's were modeled by a sum of Lorentzians multiplied by the Fermi-Dirac function. This sum is then convolved with a Gaussian representing the instrument resolution. The band dispersions extracted from the modeling are shown as filled circles in Fig. 3(c). Figure 4 shows an example of the modeling results.

As can be seen in Fig. 3(c), band 0 is extremely flat. Its energy was pinned at the experimental Fermi level, which was derived from a clean platinum foil in electrical contact with the sample. This band is the donor impurity band, which resides in the narrow band gap ($E_g \approx 0.15$ eV) of the intrinsic material. Band 1 is the highest valence band. Along this symmetry line it reaches a maximum energy at approximately $1/2\overline{\Gamma Z}$ and disperses toward higher binding energies to either side of the local maximum. Bands 2 through 6 are quite flat showing very little dispersion. The lack of dispersion in the bands in the k_z direction indicates that the material behaves quasi-two dimensionally. The high degree of anisotropy is also found in transport measurements.[22]

Shown in Fig. 3(a) are the band dispersions for intrinsic Bi_2Te_3 along Γ-*Z* as calculated by Larson, Mahanti and Kanatzidis[10] using the self-consistent full-potential linearized augmented plane wave method with spin-orbit interactions included. The calculation results of Mishra, Satpathy, and Jepsen[11] are similar. Within 3.5 eV below E_{VBM} Larson, Mahanti, and Kanatzidis find nine valence bands. The calculation shows the top valence band well separated from the lowest conduction band, with a local maximum around $1/2\overline{\Gamma Z}$. Although this band has the same dispersion trend as that of the observed one, it has a significantly higher binding energy. The calculated bands along this direction have dispersions of 0.3–0.5 eV, compared to the small dispersions (less than 0.1 eV) in the observed bands 2 through 6.

Figure 2(b) shows the off-normal emission EDC's taken for *k* points along the Γ-*a*-*U* line from an *n*-type sample. The photon energy ($h\nu$) and the polar angle (θ) are varied

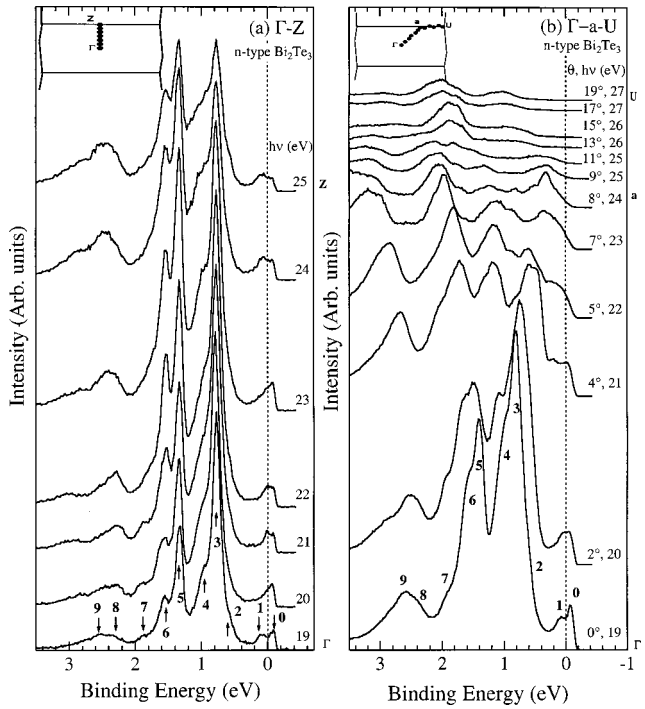

FIG. 2. Energy distribution curves (EDC's) for an *n*-type Bi_2Te_3 sample taken along (a) Γ-*Z* (normal emission) and (b) Γ-*a*-*U* (off-normal emission). The corresponding *k* points are shown in the insets. The energy is referenced to the valence-band maximum (see the text).

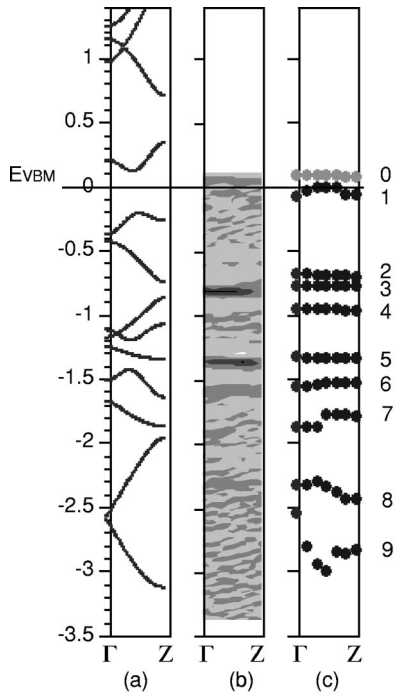

FIG. 3. (a) Band dispersions along Γ-*Z* from band-structure calculations by Larson *et al.*[10] (b) The intensity plot of the second derivatives of the EDC's ($\partial^2 I/\partial E^2$) as a function of energy and *k* in a linear-gray scale with dark corresponding to high intensity. (c) Band dispersions extracted from spectral modeling (see the text). The diameter of the symbol is approximately the energy resolution.

simultaneously to reach the desired *k* points,[20] which are shown in the inset. Again, the energy is referenced to the valence-band maximum E_{VBM}. Figures 5(a)–5(c) show the band dispersions along Γ-*a*-*U* as calculated by Larson, Mahanti, and Kanatzidis,[10] the intensity plot of the second derivative of the measured spectra, and the band dispersions extracted from spectral modeling (filled circles), respectively. The calculation shows nine very dispersive valence bands. In contrast to the bands along Γ-*Z*, which have dispersions of 0.3–0.5 eV, bands along this direction have dispersions as large as 1.5 eV. The top valence band reaches a maximum near the point ''*a*,'' which is also the absolute maximum of the valence bands. A VBM along Γ-*a*-*U* implies that it is sixfold degenerate in *k* space. This result is consistent with the result of the dHvA and SdH experiments.[12–15]

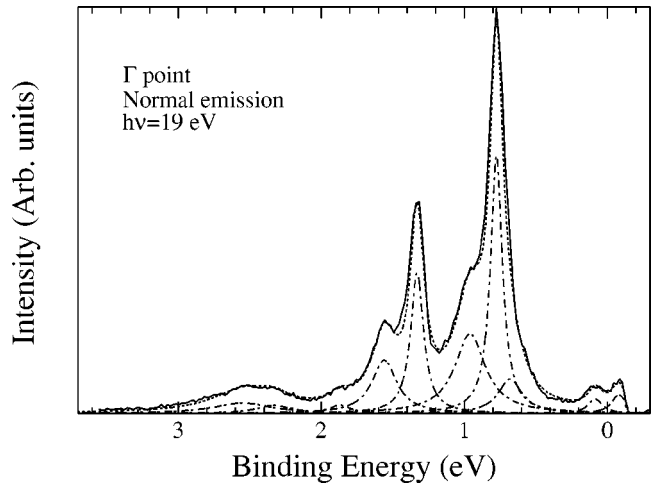

FIG. 4. An example of the spectral modeling (see the text) results. The spectrum was taken at Γ. The solid line is the measured data; the dotted line is the modeling result; the dot-dashed lines are the individual Lorentzian peaks used in the modeling.

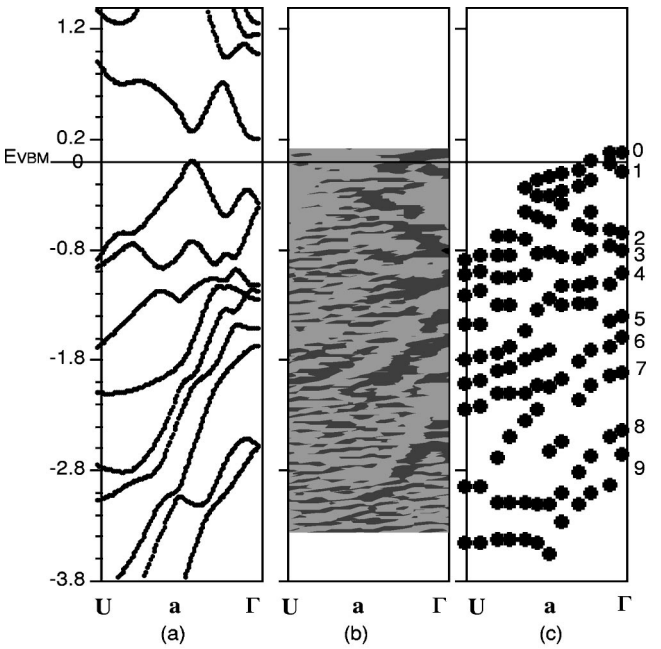

FIG. 5. (a) Band dispersions along Γ-*a*-*U* from band-structure calculation by Larson, Mahanti, and Kanatzidis.[10] (b) The intensity plot of the second derivatives of the EDC's ($\partial^2 I/\partial E^2$) as a function of energy and *k*. (c) Band dispersions extracted from spectral modeling. The diameter of the symbol is approximately the energy resolution.

In our experiment, we observed ten bands in an *n*-type sample [labeled 0 through 9 in Fig. 5(c)]. Band 0 is the donor impurity band which is nondispersive and its energy was pinned at the Fermi level reference. It is localized around the Γ point, disappearing within 12% of $\overline{\Gamma aU}$ from Γ. The remaining nine bands are highly dispersive. Band 1, which is the highest valence band, reaches a maximum at approximately 20% of $\overline{\Gamma aU}$ from Γ. It then disperses toward higher binding energy and converges with lower bands, becoming barely visible after the point *a*. This dispersion is quite different from that of the calculation that shows the top valence band to have two local maxima, one near the Γ point (approximately 10% of $\overline{\Gamma aU}$ from Γ), the other near the *a* point (approximately 40% of $\overline{\Gamma aU}$ from Γ) the latter being the absolute maximum. The theoretical calculations of the effective-mass tensor associated with the VBM agree very well with dHvA results. Note that dHvA measurements do not give the position of the maximum. Furthermore, band 2, the second highest valence band, is separated by ~600 meV from band 1 at the Γ point. It disperses toward lower binding energy and reaches a maximum near the point *a*, after which its intensity diminishes. This dispersion behavior is also very different from that of the calculation. The remaining valence bands appear to have qualitative correspondence with theory although it is difficult to trace the dispersion of each band given the high density of bands in this material and their complicated structure.

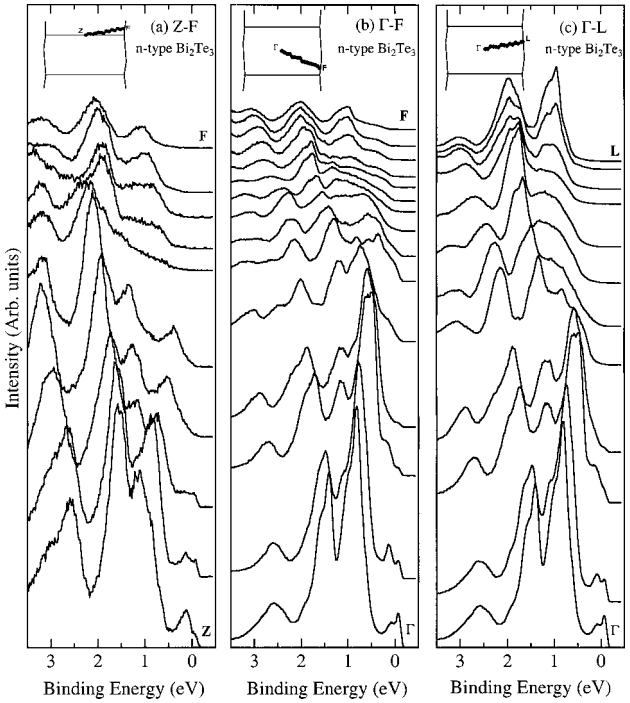

FIG. 6. EDC's for an *n*-type Bi_2Te_3 sample taken along (a) *Z*-*F*, (b) Γ-*F*, and (c) Γ-*L*. The corresponding *k* points are shown in the insets. The energy is referenced to the valence-band maximum.

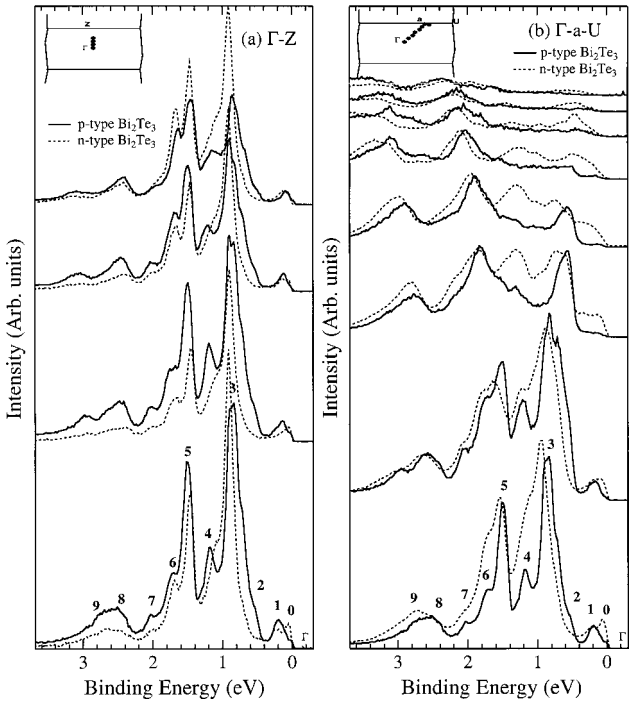

FIG. 7. EDC's for a *p*-type Bi_2Te_3 sample (solid lines) taken along (a) Γ-*Z* (normal emission) and (b) Γ-*a*-*U* (off-normal emission). The corresponding *k* points are shown in the insets. The energy is referenced to the experimental Fermi level reference derived from a clean platinum foil in electrical contact with the sample. The EDC's for an *n*-type sample are also shown (dashed lines) for comparison.

Spectra from the *n*-type sample were also taken along the three other symmetry lines *Z*-*F*, Γ-*F*, and Γ-*L*. They are shown in Figs. 6(a), 6(b), and 6(c), respectively. The impurity band can be seen near the *Z* and Γ points. The valence bands are quite dispersive along these directions. The top valence band disperses toward higher binding energies away from the *Z* and Γ points, thus the VBM is not located along these directions.

The local valence-band maxima observed along Γ-*a*-*U* and Γ-*Z* are very close in energy. The maximum along Γ-*a*-*U* is slightly higher than the one along Γ-*Z*. Thus the maximum along Γ-*a*-*U* is the absolute VBM. However, the difference is small, being only ~30 meV, which is smaller than our experimental resolution. Higher resolution measurements should make a better distinction. A VBM along Γ-*a*-*U* is consistent with both band-structure calculations and SdH and dHvA experiments.

Shown in Figs. 7(a) and 7(b) are the EDC's from a *p*-type sample (solid lines) for *k* points along Γ-*Z* and Γ-*a*-*U*, respectively. The initial energy is referenced to the experimental Fermi level reference derived from a clean platinum foil in electrical contact with the sample. EDC's from the *n*-type sample are superimposed (dashed lines, also referenced to the experimental Fermi level) for comparison. As can be seen, the spectra from the *p*- and *n*-type samples have rather similar spectral features. The main differences between the two are: (1) the impurity band in the *p*-type sample (labeled as band 0) is seen only as a tail, which is expected because the chemical potential for a *p*-type semiconductor lies just below the impurity level and (2) the top few valence bands (band 1 through 4) are shifted toward lower binding energy (by approximately 0.095 eV for band 1, and 0.2 eV for bands 2–4) in the *p*-type sample relative to those in the *n*-type sample. The amount of shift is on the order of the band gap and the direction of the shift is consistent with the *p*-type doping. The remaining bands, 5 through 9, appear to be not shifted. This may be due to the fact that the *p*-type sample is substitutionally doped with excess bismuth which occupies the tellurium sites. The calculation by Larson, Mahanti, and Kanatzidis[10] shows that along the Γ-*a*-*U* line, the top valence bands have predominantly tellurium character and so would be more affected by the loss or addition of tellurium in the crystal. Along the Γ-*Z* line, the calculation finds that the top valence band is a Bi-Te hybridized band. The hybridization is caused by the inclusion of the spin-orbit interaction, which also pulls the top valence band towards higher binding energies.

To summarize, we find that the VBM in Bi_2Te_3 is located along the Γ-*a*-*U* line and therefore is sixfold degenerate in *k* space. This is consistent with the result of the band-structure calculation.[10] However, we also find some discrepancies between our data and the calculation results. The position of the VBM along Γ-*a*-*U* is different. Also, we find that the bands along Γ-*Z* have minimal dispersions (<0.1 eV), compared to the larger dispersions (0.3–0.5 eV) predicted by the calculation. Possible reasons for this discrepancy are the disorder caused by the dopants, the electron-phonon interaction, and the electron-electron interaction. These three effects could cause band narrowing. The flat bands along Γ-*Z* could generate carriers with large effective masses along this direction which, coupled with the high degeneracy of the bands

along the *ab* plane of the crystal, can explain the remarkable thermoelectric properties of Bi_2Te_3.[23] Also, we did not observe the increase of binding energy in the top valence band along Γ-Z due to spin-orbit interaction. Finally, these observations indicate that the subtle details of the electronic structure of Bi_2Te_3 are not fully understood and illustrate the need for further investigation.

The authors thank Dr. S. D. Mahanti and P. Larson for many helpful discussions. This work was partially supported by the NSF under award No. DMR9801776, and by the Center for Fundamental Materials Research, Michigan State University. This work was based upon research conducted at the Synchrotron Radiation Center, University of Wisconsin, Madison, which was supported by the NSF under Award No. DMR9531009. Ames Laboratory is operated for the U.S. D.O.E. by Iowa State University under Contract No. W-7405-ENG-82. Two of the authors (D.Y.C. and M.G.K.) were supported by the Office of Naval Research Grant No. N00014-98-1-0443.

[1] The performance of a thermoelectric material is characterized by a dimensionless figure of merit $ZT=(\sigma S^2 T)/\kappa$, where S is the thermopower, T is the temperature, σ is the electrical conductivity, and κ is the thermal conductivity (see Refs. 2 and 3). Bi_2Te_3 is the best room temperature thermoelectric material found to date with a $ZT\approx 1$ (see Refs. 2 and 5).

[2] G. Mahan, B. Sales, and J. Sharp, Phys. Today **50**, 42 (1997).

[3] G. A. Slack, in CRC *Handbook of Thermoelectrics*, edited by D. M. Rowe (CRC Press, Boca Raton, FL, 1995), Chap. 34.

[4] F. J. DiSalvo, Science **285**, 703 (1999).

[5] H. J. Goldsmid, *Electronic Refrigeration* (Pion, London, 1986).

[6] The degree of *k*-space degeneracy here refers to the number of equivalent locations in the three-dimensional Brillouin zone due to symmetry.

[7] There is one previous ARPES experiment on Bi_2Te_3 with low-resolution [R. L. Benbow and Z. Hurych, Solid State Commun. **28**, 641 (1978)], and one angle integrated photoemission experiment [Y. Ueda, A. Furata, H. Okuda, M. Nakatake, H. Sato, H. Namatame, and M. Taniguchi, J. Electron Spectrosc. Relat. Phenom. **101-103**, 677 (1999)].

[8] M. G. Kanatzidis and F. J. DiSalvo, ONR Quarterly Rev. **47**, 14 (1996).

[9] D.-Y. Chung, T. Hogan, P. Brasis, M. Rocci-Lane, C. Kannewurf, M. Bastea, C. Uher, and M. G. Kanatzidis, Science **287**, 1024 (2000).

[10] P. Larson, S. D. Mahanti, and M. G. Kanatzidis, Phys. Rev. B **61**, 8162 (2000).

[11] S. K. Mishra, S. Satpathy, and O. Jepsen, J. Phys.: Condens. Matter **9**, 461 (1997).

[12] R. B. Mallinson, J. A. Rayne, and R. W. Ure, Jr., Phys. Rev. **175**, 1049 (1968).

[13] L. R. Testardi, P. J. Stiles, and E. Burstein, Solid State Commun. **1**, 28 (1963).

[14] H. Kohler, Phys. Status Solidi B **73**, 95 (1976).

[15] H. Kohler, Phys. Status Solidi B **74**, 591 (1976).

[16] G. A. Thomas, D. H. Rapke, R. B. Van Dover, L. F. Mattheis, W. A. Surden, L. F. Schneemaper, and J. V. Waszczak, Phys. Rev. B **46**, 1553 (1992).

[17] R. W. G. Wyckoff, *Crystal Structures* (Krieger, London, 1986), Vol. 2.

[18] B. Schroeder, A. Von Middendorff, H. Kohler, and G. Landwehr, Phys. Status Solidi B **59**, 561 (1973).

[19] S. N. Chizhevskaya and L. E. Shelimova, Inorg. Mater. (Transl. of Neorg. Mater.) **31**, 1083 (1995).

[20] For normal emission data, the *k* values were calculated using the formula $k_\perp=[2m(E_K+V_0)/\hbar^2]^{1/2}$, where E_K is the kinetic energy of the photoelectron and V_0 is the inner potential which was experimentally determined to be 10 eV. This formula is obtained by assuming a free-electron approximation for the final-state band structure. For off-normal emission data, *k* values can be calculated using $k_\parallel=[2mE_K/\hbar^2]^{1/2}\sin\theta$ and $k_\perp=[2m(E_K+V_0-E_K\sin^2\theta)/\hbar^2]^{1/2}$. For more detail, see T. C. Chiang, J. A. Knapp, M. Aono, and D. E. Eastman, Phys. Rev. B **21**, 3513 (1980).

[21] F. J. Himpsel, Adv. Phys. **32**, 1 (1983).

[22] A. E. Karkin, V. V. Shchennikov, B. N. Goshchitskii, S. E. Danilov, and V. L. Arbuzov, Zh. Phys. Teor. Fiz. **113**, 1787 (1998) [Sov. Phys. JETP **86**, 976 (1998)].

[23] This is based on the B parameter $B=T^{5/2}\gamma(m_x m_y m_z)^{1/2}(\mu_x/\kappa_L)$, where m_x, m_y, m_z are the effective masses in the x, y, z directions, respectively, μ_x is the carrier mobility along the x direction, γ is the band degeneracy, and κ_L is the lattice thermal conductivity, as discussed by L. D. Hicks and M. S. Dresselhaus, Phys. Rev. B **47**, 12 727 (1993).